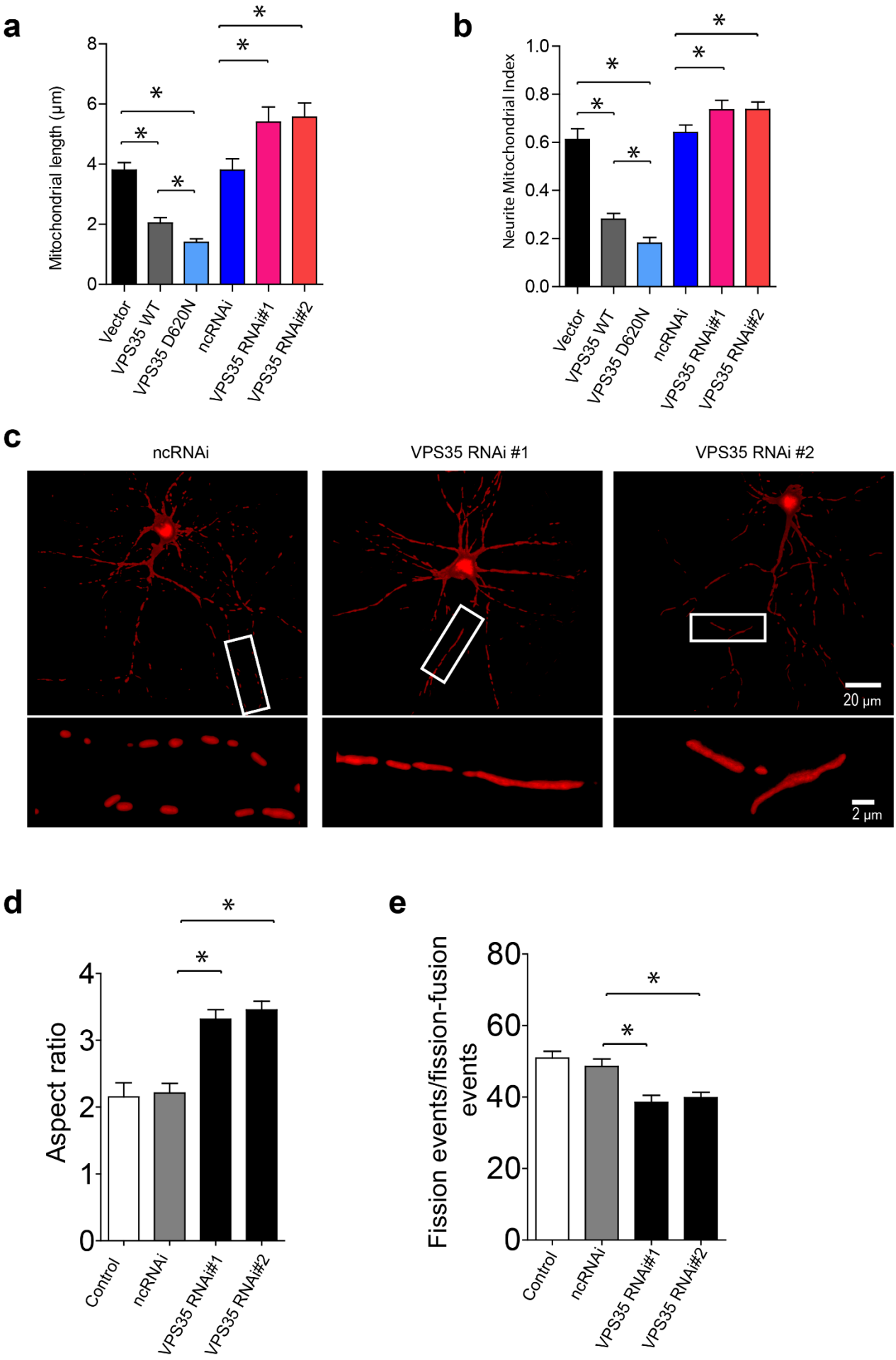
a
Mitochondrial length (μm)
0
2
4
6
8
*
*
*
*
*
Vector
VPS35 WT
VPS35 D620N
ncRNAi
VPS35 RNAi#1
VPS35 RNAi#2
b
Neurite Mitochondrial Index
0.0
0.2
0.4
0.6
0.8
1.0
*
*
*
*
*
Vector
VPS35 WT
VPS35 D620N
ncRNAi
VPS35 RNAi#1
VPS35 RNAi#2
c
ncRNAi
VPS35 RNAi #1
VPS35 RNAi #2
20 μm
2 μm
d
Aspect ratio
0
1
2
3
4
*
*
Control
ncRNAi
VPS35 RNAi#1
VPS35 RNAi#2
e
Fission events/fission-fusion events
0
20
40
60
80
*
*
Control
ncRNAi
VPS35 RNAi#1
VPS35 RNAi#2

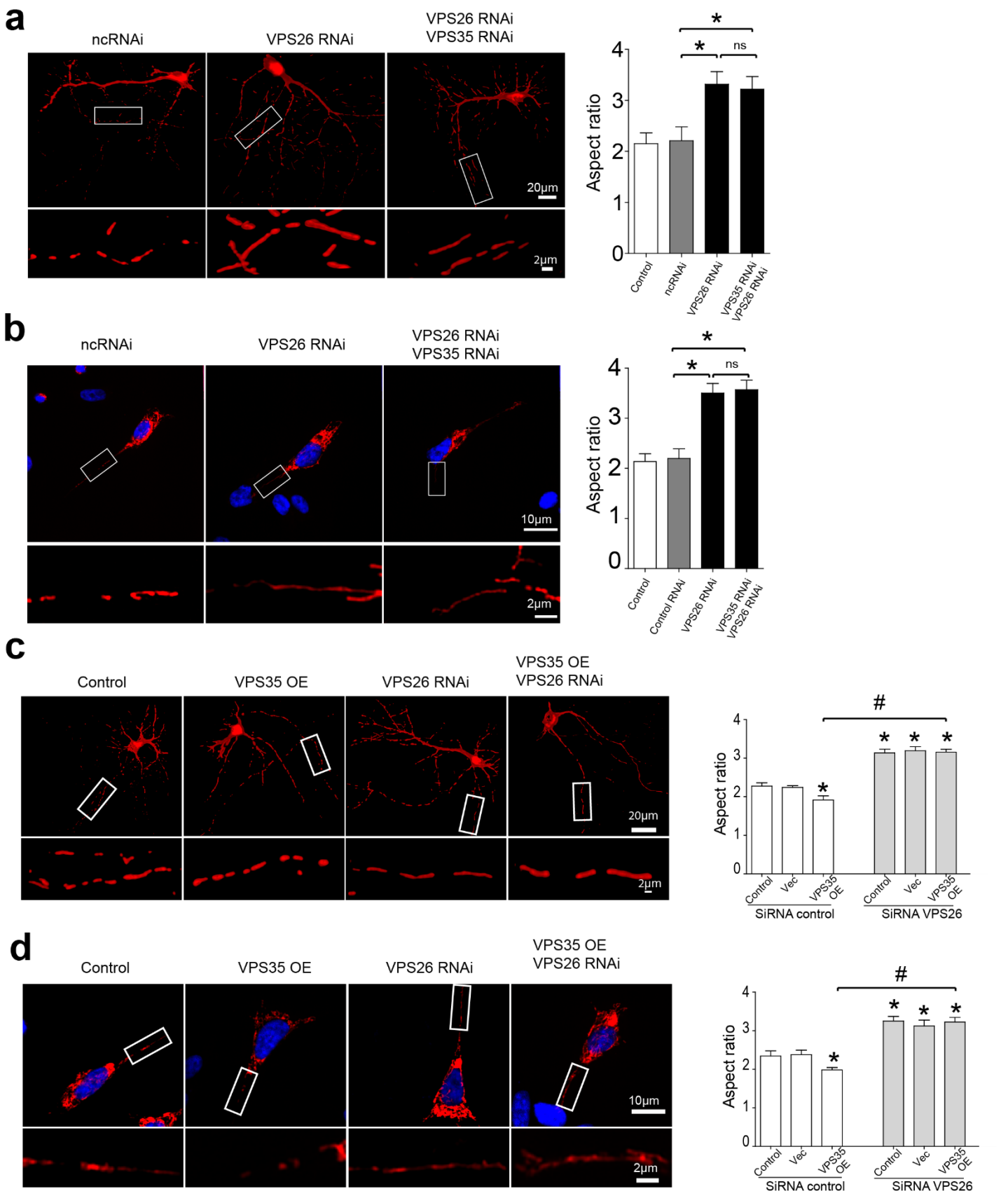
a
ncRNAi
VPS26 RNAi
VPS26 RNAi
VPS35 RNAi
20μm
2μm
Aspect ratio
ns
Control
ncRNAi
VPS26 RNAi
VPS35 RNAi
VPS26 RNAi
b
ncRNAi
VPS26 RNAi
VPS26 RNAi
VPS35 RNAi
10μm
2μm
Aspect ratio
ns
Control
Control RNAi
VPS26 RNAi
VPS35 RNAi
VPS26 RNAi
c
Control
VPS35 OE
VPS26 RNAi
VPS35 OE
VPS26 RNAi
20μm
2μm
Aspect ratio
Control
Vec
VPS35 OE
Control
Vec
VPS35 OE
SiRNA control
SiRNA VPS26
d
Control
VPS35 OE
VPS26 RNAi
VPS35 OE
VPS26 RNAi
10μm
2μm
Aspect ratio
Control
Vec
VPS35 OE
Control
Vec
VPS35 OE
SiRNA control
SiRNA VPS26

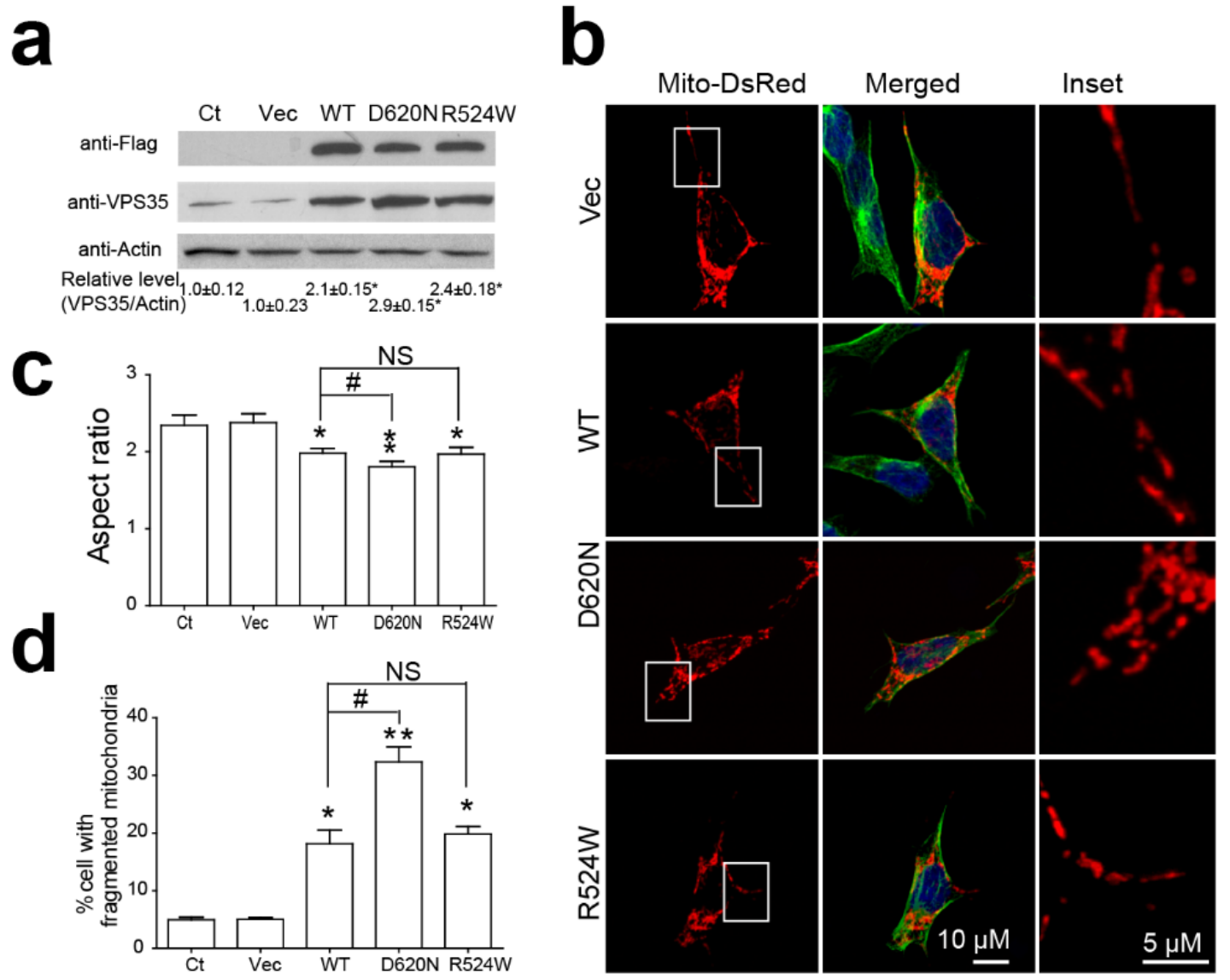
a
Ct
Vec
WT
D620N
R524W
anti-Flag
anti-VPS35
anti-Actin
Relative level
(VPS35/Actin)
1.0±0.12
1.0±0.23
2.1±0.15*
2.9±0.15*
2.4±0.18*
b
Mito-DsRed
Merged
Inset
Vec
WT
D620N
R524W
10 μM
5 μM
c
Aspect ratio
NS
#
*
**
*
Ct
Vec
WT
D620N
R524W
d
% cell with fragmented mitochondria
NS
#
**
*
*
Ct
Vec
WT
D620N
R524W

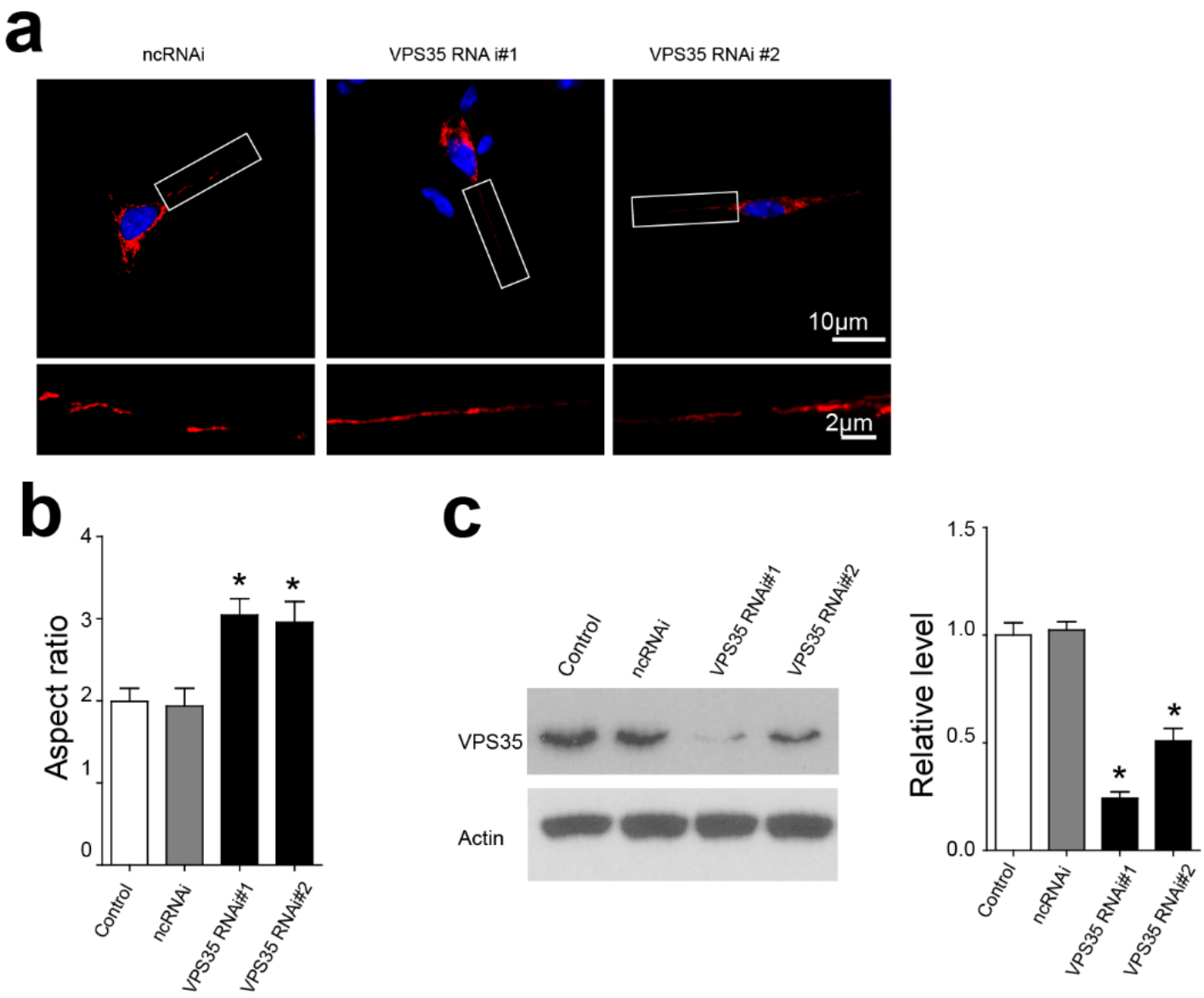
a
ncRNAi
VPS35 RNA i#1
VPS35 RNAi #2
10μm
2μm
b
Aspect ratio
4
3
2
1
0
*
*
Control
ncRNAi
VPS35 RNAi#1
VPS35 RNAi#2
c
Control
ncRNAi
VPS35 RNAi#1
VPS35 RNAi#2
VPS35
Actin
Relative level
1.5
1.0
0.5
0.0
*
*
Control
ncRNAi
VPS35 RNAi#1
VPS35 RNAi#2

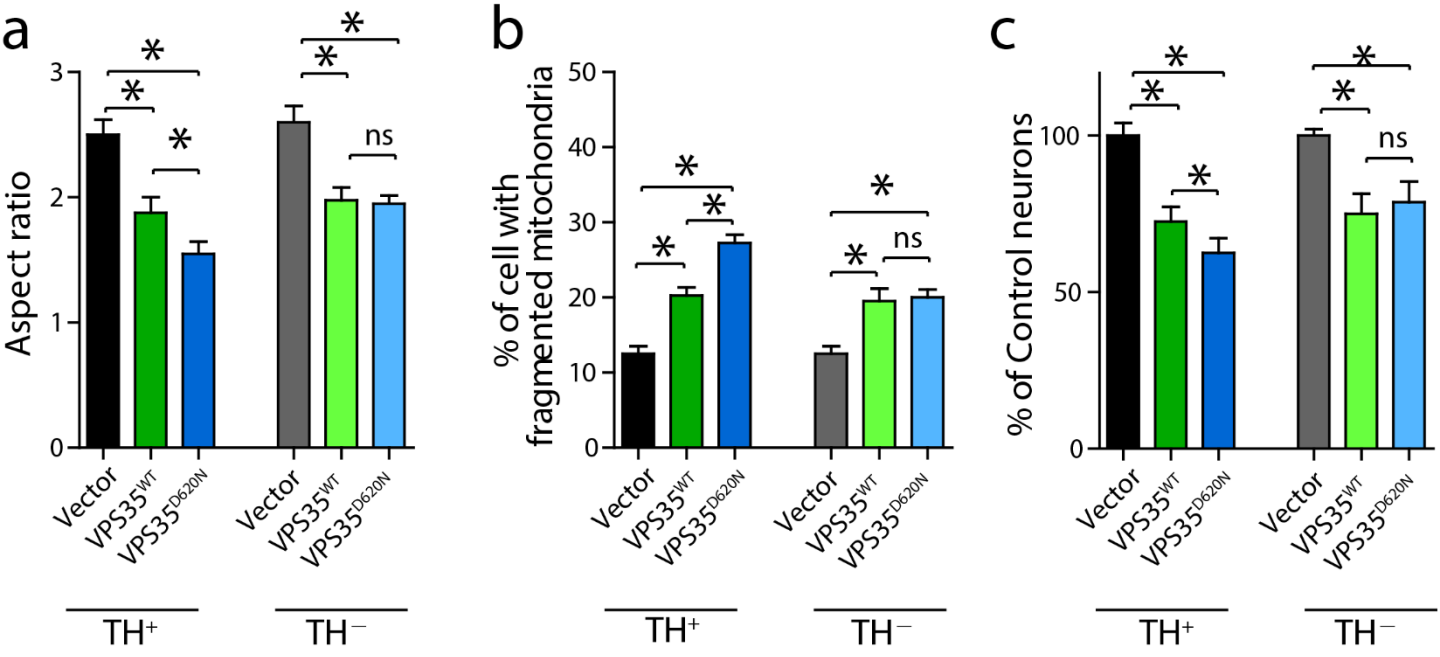
a
Aspect ratio
3
2
1
0
*
*
*
*
*
ns
Vector
VPS35WT
VPS35D620N
Vector
VPS35WT
VPS35D620N
TH+
TH−
b
% of cell with fragmented mitochondria
50
40
30
20
10
0
*
*
*
*
*
ns
Vector
VPS35WT
VPS35D620N
Vector
VPS35WT
VPS35D620N
TH+
TH−
c
% of Control neurons
100
50
0
*
*
*
*
*
ns
Vector
VPS35WT
VPS35D620N
Vector
VPS35WT
VPS35D620N
TH+
TH−

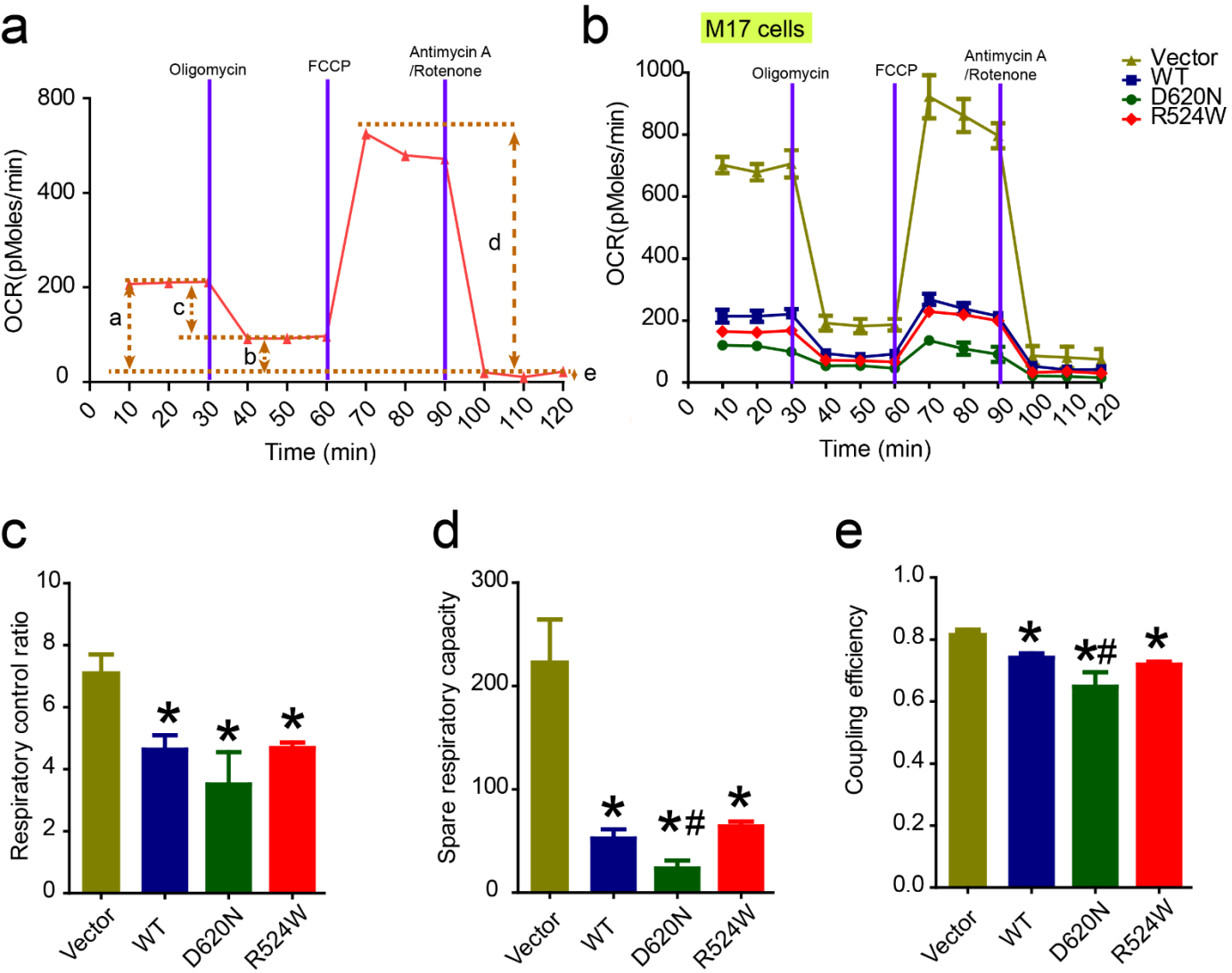
a
Oligomycin
FCCP
Antimycin A
/Rotenone
OCR(pMoles/min)
Time (min)
a
b
c
d
e
b
M17 cells
Vector
WT
D620N
R524W
c
Respiratory control ratio
d
Spare respiratory capacity
e
Coupling efficiency
Vector
WT
D620N
R524W

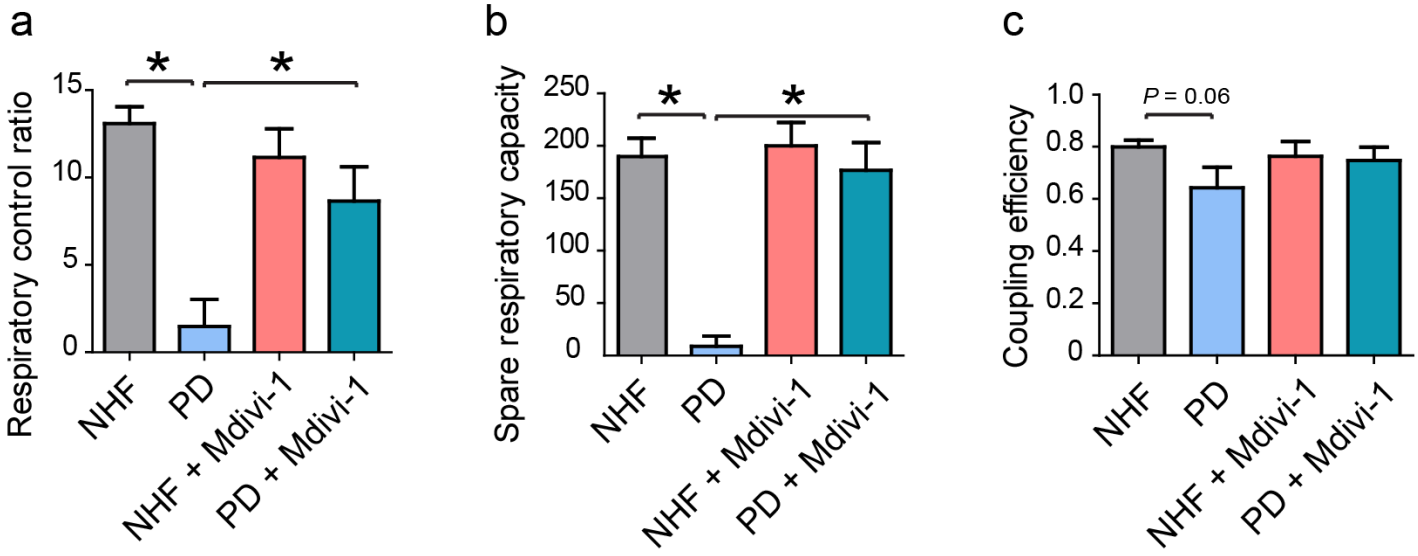
a
Respiratory control ratio
15
10
5
0
*
*
NHF
PD
NHF + Mdivi-1
PD + Mdivi-1
b
Spare respiratory capacity
250
200
150
100
50
0
*
*
NHF
PD
NHF + Mdivi-1
PD + Mdivi-1
c
Coupling efficiency
1.0
0.8
0.6
0.4
0.2
0
P = 0.06
NHF
PD
NHF + Mdivi-1
PD + Mdivi-1

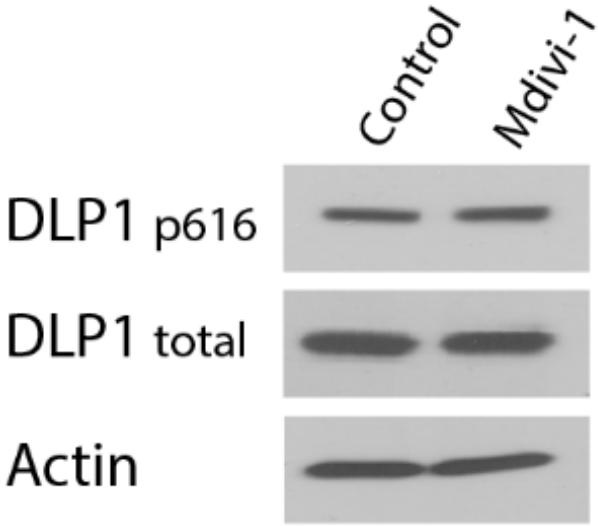
Control
Mdivi-1
DLP1 p616
DLP1 total
Actin

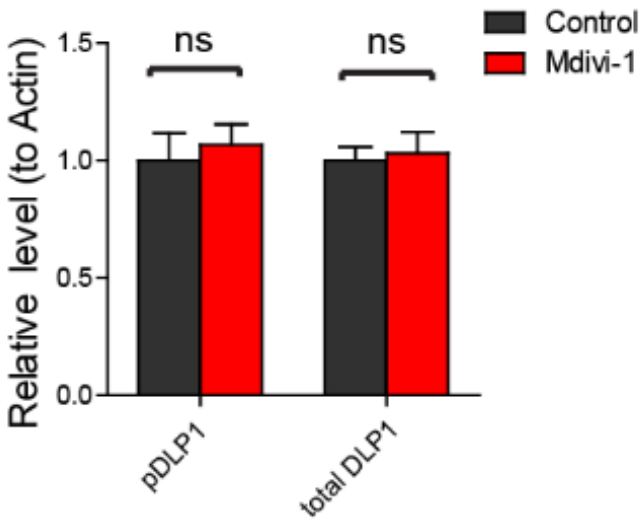
Control
Mdivi-1
Relative level (to Actin)
1.5
1.0
0.5
0.0
ns
ns
pDLP1
total DLP1

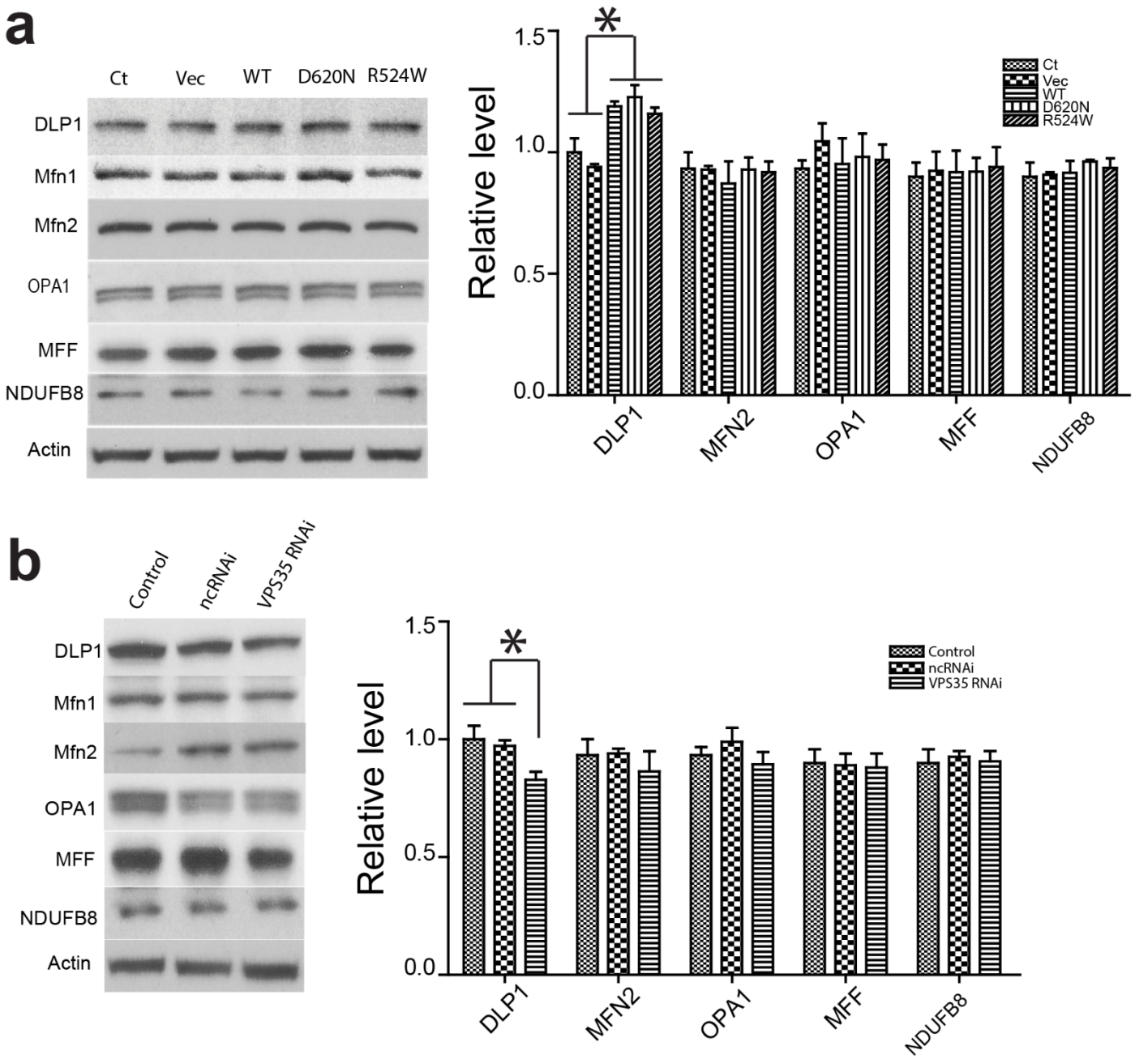
a
Ct
Vec
WT
D620N
R524W
DLP1
Mfn1
Mfn2
OPA1
MFF
NDUFB8
Actin
Relative level
1.5
1.0
0.5
0.0
*
Ct
Vec
WT
D620N
R524W
DLP1
MFN2
OPA1
MFF
NDUFB8
b
Control
ncRNAi
VPS35 RNAi
DLP1
Mfn1
Mfn2
OPA1
MFF
NDUFB8
Actin
Relative level
1.5
1.0
0.5
0.0
*
Control
ncRNAi
VPS35 RNAi
DLP1
MFN2
OPA1
MFF
NDUFB8

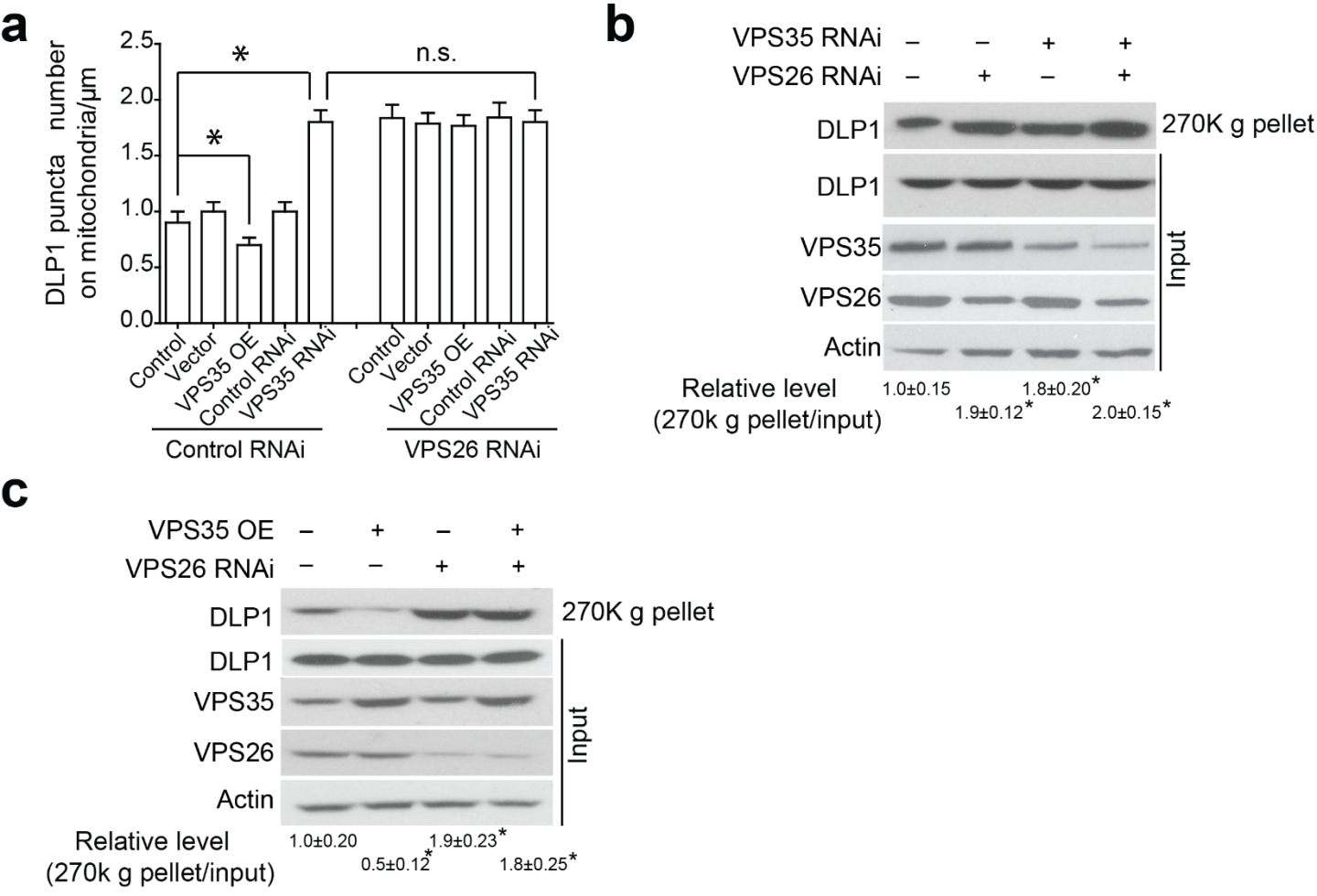
a
DLP1 puncta number on mitochondria/μm
2.5
2.0
1.5
1.0
0.5
0.0
*
*
n.s.
Control
Vector
VPS35 OE
Control RNAi
VPS35 RNAi
Control
Vector
VPS35 OE
Control RNAi
VPS35 RNAi
Control RNAi
VPS26 RNAi
b
VPS35 RNAi – – + +
VPS26 RNAi – + – +
DLP1
DLP1
VPS35
VPS26
Actin
270K g pellet
Input
Relative level
(270k g pellet/input)
1.0±0.15
1.9±0.12*
1.8±0.20*
2.0±0.15*
c
VPS35 OE – + – +
VPS26 RNAi – – + +
DLP1
DLP1
VPS35
VPS26
Actin
270K g pellet
Input
Relative level
(270k g pellet/input)
1.0±0.20
0.5±0.12*
1.9±0.23*
1.8±0.25*

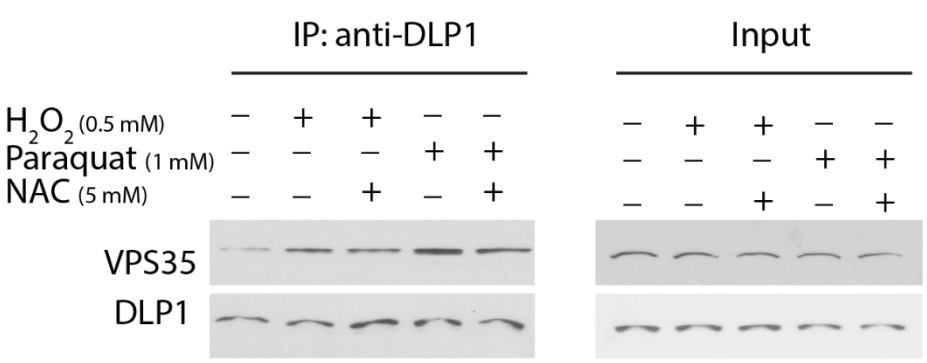
IP: anti-DLP1
Input
H2O2 (0.5 mM)
Paraquat (1 mM)
NAC (5 mM)
VPS35
DLP1

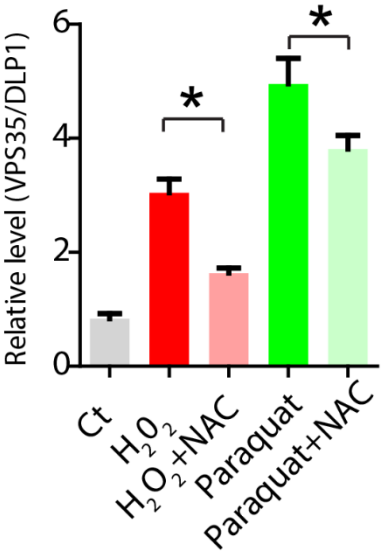
Relative level (VPS35/DLP1)
0
2
4
6
*
*
Ct
H2O2
H2O2+NAC
Paraquat
Paraquat+NAC

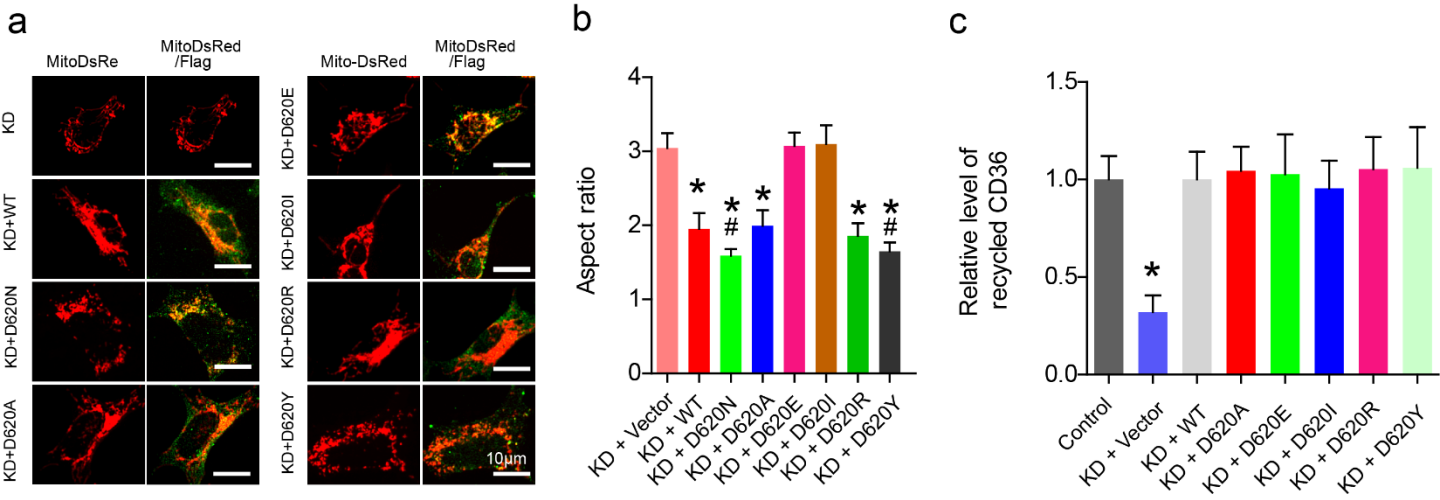
a
MitoDsRe
MitoDsRed /Flag
Mito-DsRed
MitoDsRed /Flag
KD
KD+WT
KD+D620N
KD+D620A
KD+D620E
KD+D620I
KD+D620R
KD+D620Y
10μm
b
Aspect ratio
0
1
2
3
4
KD + Vector
KD + WT
KD + D620N
KD + D620A
KD + D620E
KD + D620I
KD + D620R
KD + D620Y
c
Relative level of recycled CD36
0.0
0.5
1.0
1.5
Control
KD + Vector
KD + WT
KD + D620A
KD + D620E
KD + D620I
KD + D620R
KD + D620Y

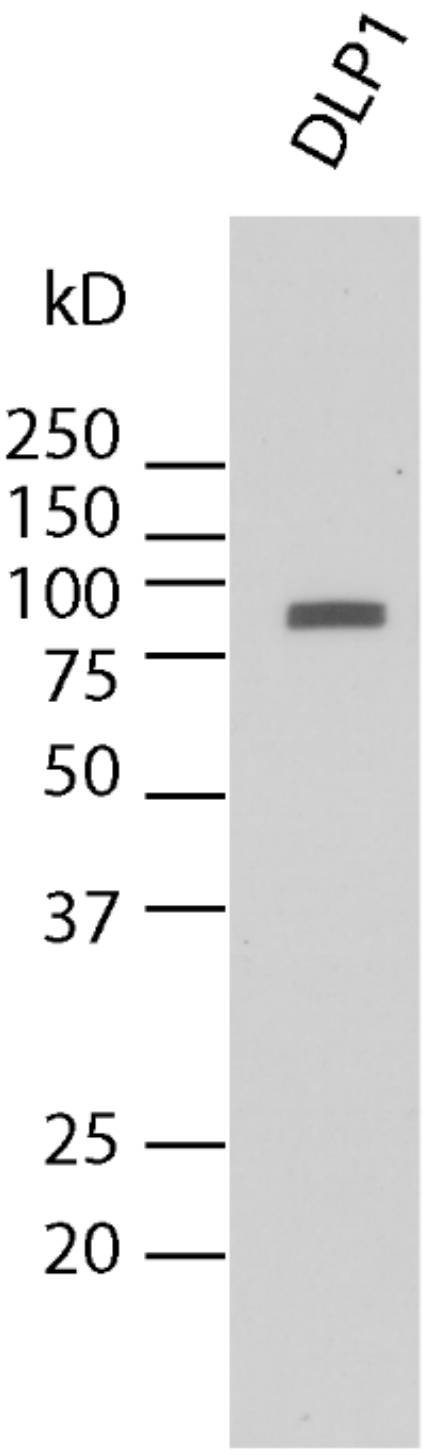
DLP1
kD
250
150
100
75
50
37
25
20

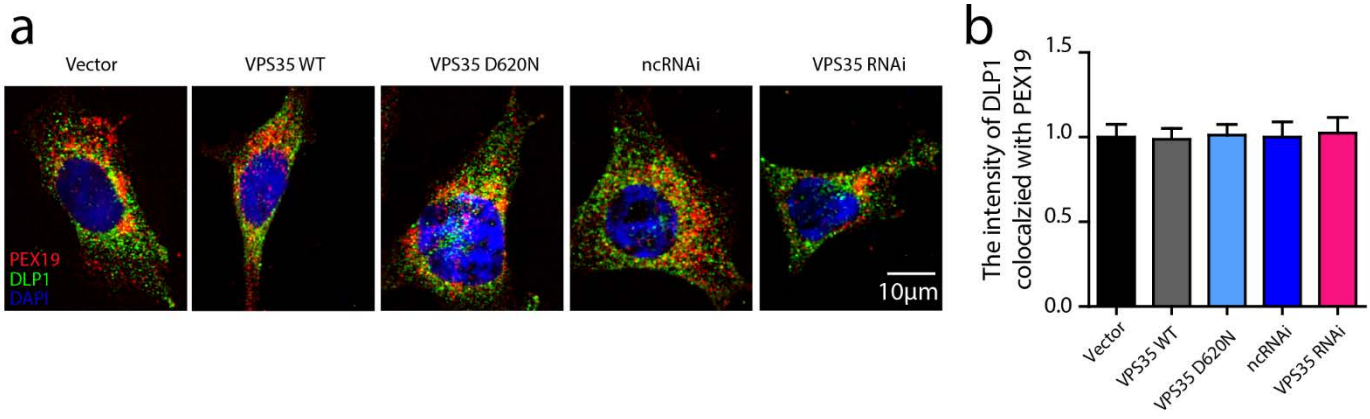
a
Vector
VPS35 WT
VPS35 D620N
ncRNAi
VPS35 RNAi
PEX19
DLP1
DAPI
10μm
b
The intensity of DLP1 colocalzied with PEX19
1.5
1.0
0.5
0.0
Vector
VPS35 WT
VPS35 D620N
ncRNAi
VPS35 RNAi

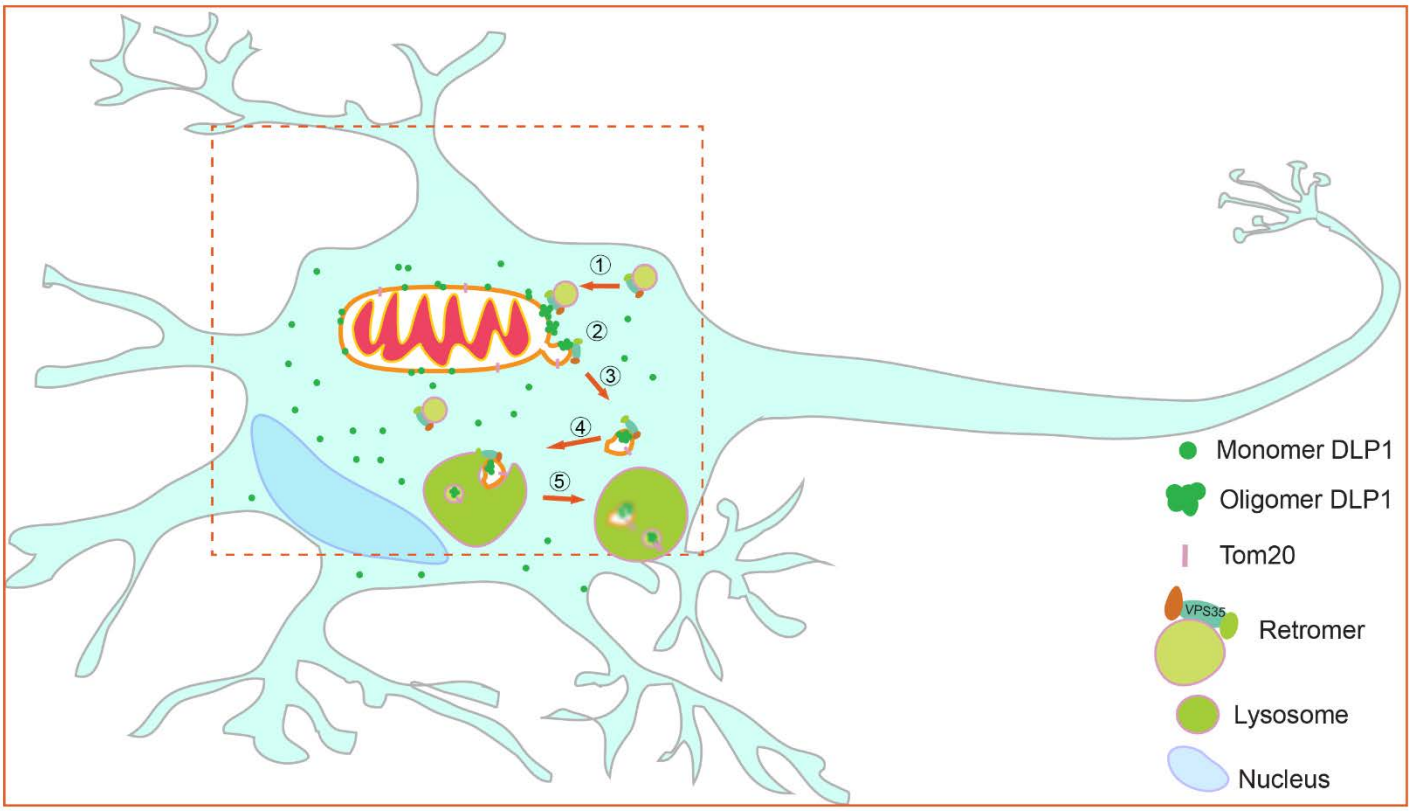
①
②
③
④
⑤
Monomer DLP1
Oligomer DLP1
Tom20
VPS35
Retromer
Lysosome
Nucleus

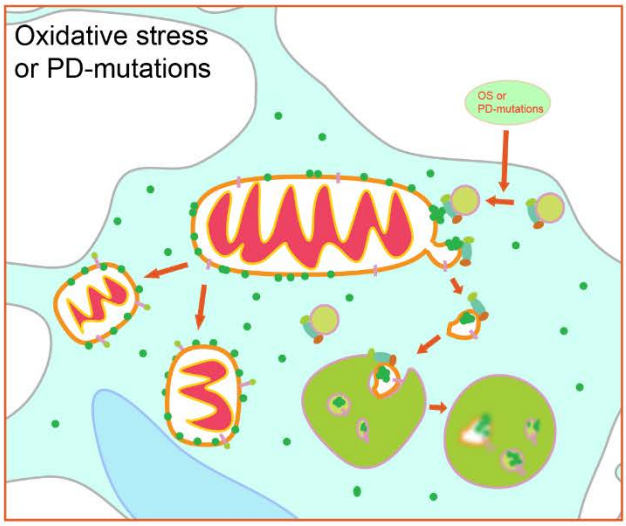
Oxidative stress
or PD-mutations
OS or
PD-mutations

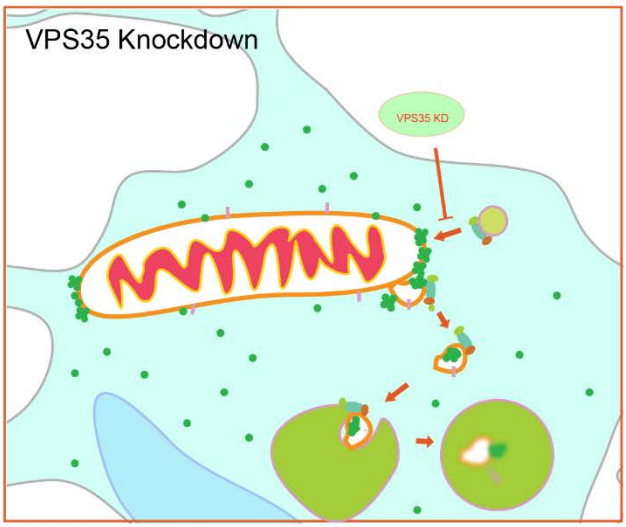
VPS35 Knockdown
VPS35 KD

Figure Legends for Supplementary Figures

Supplementary Figure 1. VPS35 overexpression and knockdown cause opposite changes in mitochondrial dynamics in primary cortical neurons. Primary rat cortical neurons were co-transfected with constructs encoding flag-tagged VPS35 (WT or D620N) or GFP-tagged miR RNAi expression vectors targeting VPS35 and mitoDsRed2 at DIV7 and imaged at DIV9 to analyze mitochondrial dynamics. Mitochondrial length (**a**) and the neurite mitochondrial index (**b**) in the axon were quantified in the same neurons analyzed in (**Fig. 1b,c**). (**c**) Representative 3D confocal images of mitochondria in primary rat cortical neurons expressing GFP-tagged-VPS35 RNAi and mitoDsRed2. (**d**) Quantification of aspect ratio of mitochondria in primary rat cortical neurons expressing GFP-tagged-VPS35 RNAi and mitoDsRed2. (**e**) Ratio of fission over fission-plus-fusion events of mitochondria in live cultured primary rat cortical neurons expressing GFP-tagged-VPS35 RNAi and mitoDsRed2. Data are means ± SEM from three independent experiments. Statistics: one-way analysis of variance (ANOVA) followed by Tukey's multiple comparison test. * $P < 0.05$, compared to control neuron.

Supplementary Figure 2. VPS26 and VPS35 act through the same pathway in the regulation of mitochondrial dynamics. (**a**) Representative 3D confocal images of mitochondria (left panel) and quantification of mitochondrial aspect ratio (right panel) in primary rat cortical neurons co-transfected with indicated RNAi and mitoDsRed2. *$P <$ 0.05, ns, not significant. (**b**) Representative confocal images of mitochondria (left panel) and quantification of mitochondrial aspect ratio (right panel) in M17 stable cell lines (ncRNAi or VPS35 RNAi) transiently-transfected with indicated VPS26 RNAi and mitoDsRed2. *$P <$ 0.05, ns, not significant. (**c**) Representative 3D confocal images of mitochondria (left panel) and quantification of mitochondrial aspect ratio (right panel) in primary rat cortical neurons co-transfected with VPS26 RNAi and/or WT VPS35 constructs and mitoDsRed2. *$P < 0.05$, compared with control + siRNA control and vec + siRNAi control; # $P <0.05$, (**d**) Representative confocal images of mitochondria (left panel) and quantification of mitochondrial aspect ratio (right panel) in M17 stable cell lines [empty-vector (Vec) or WT VPS35 (VPS35 OE)] transiently transfected with VPS26 RNAi and mitoDsRed2. *$P < 0.05$, compared with control + siRNA control and vec + siRNAi control; # $P <0.05$, Data are means ± SEM from three independent experiments.

Statistics: one-way analysis of variance (ANOVA) followed by Tukey's multiple comparison test.

Supplementary Figure 3. VPS35 overexpression causes mitochondrial fragmentation in M17 stable cell lines. Three independent stable clonal lines overexpressing comparable levels of VPS35 for each construct (WT, D620N, and R524W) were generated and analyzed. (**a**) Representative western blot and quantification of VPS35 in M17 stable cell lines overexpressing flag-tagged WT or mutant VPS35. * $P < 0.05$, compared with normal M17 cells (Ct) and empty-vector control (Vec). Representative images (**b**) and quantification of mitochondria aspect ratio (**c**) and the percentage of neurons with fragmented mitochondria (**d**) in three independent stable M17 cell lines expressing empty-vector (Vec) or flag-tagged WT or mutant VPS35. M17 cells were transfected with mitoDsRed2 to label mitochondria and fixed for imaging 2 days after transfection. Green, tubulin; red, mitoDsRed2; blue, DAPI. Insets show enlargements of boxed areas. * $P < 0.05$, ** $P < 0.01$, compared with Ct (normal M17 cells) or Vec (empty-vector control) cells and $^{\#}$ $P < 0.05$, compared with WT VPS35 M17 cells (WT). NS, not significant. Data are means ± SEM from three independent experiments. Statistics: one-way analysis of variance (ANOVA) followed by Tukey's multiple comparison test.

Supplementary Figure 4. VPS35 Knockdown causes mitochondria elongation in M17 stable cell lines. VPS35 expression was knocked down by two different VPS35 miR-based RNAi constructs (#1 and #2). (**a**) Representative 3D confocal images of mitochondria in M17 stable cell lines transfected with miR RNAi expression vector targeting VPS35 (VPS35 KD M17 cells) and mitoDsRed2. Insets show enlargements of boxed areas. Blue: DAPI. ncRNAi, negative-control RNAi. (**b**) Quantification of mitochondrial aspect ratio as an index for mitochondrial length in three independent stable VPS35 KD M17 cells for each construct. (**c**) Representative western blot and quantification of VPS35 confirmed reduced expression in VPS35 KD M17 cells. Data are means ± SEM from three independent experiments. Statistics: one-way analysis of variance (ANOVA) followed by Tukey's multiple comparison test. * $P < 0.05$ compared to normal M17 cells (control) and ncRNAi controls.

Supplementary Figure 5. VPS35 regulates mitochondrial dynamics in C57BL/6J mice *in vivo*. 2–3 months old C57BL/6J mice were stereotactically injected with lentivirus encoding lenti-VPS35-p2a-mitoDsRed virus (*n* = 4 mice/group) unilaterally into the ventral tegmental area (VTA) and mitochondria and neurons were analyzed three weeks later. Quantification of mitochondria aspect ratio (**a),** the percentage of neurons with fragmented mitochondria (**b**) and neuronal loss (**c**) in both TH-positive and TH-negative neurons in injected C57BL/6J mice. Data are means ± SEM. Statistics: one-way analysis of variance (ANOVA) followed by Tukey's multiple comparison test. * $P < 0.05$. NS, not significant.

Supplementary Figure 6. VPS35 overexpression causes bioenergetic defects in M17 cells. Using a seahorse XF24 analyzer, oxygen consumption rate (OCR) was measured in M17 cells being sequentially exposed to control medium, oligomycin (inhibits ATP synthase, blocks oxygen consumption related to ATP synthesis), FCCP (uncoupler to assess maximal OCR), and antimycin A/rotenone (blocks electron flux through both complex I and II). (**a**) Expected response in OCR as cells were treated with each successive compound[22]. *a*, basal respiration; *b*, oligomycin-insensitive (leak) respiration; *c*, ATP-dependent respiration; *d*, maximal respiration, *e*, non-mitochondrial respiration. Derived parameters: respiratory control ratio (*d/b*); spare respiratory capacity (*d-a*) and coupling efficiency (*c/a*). (**b**) The representative OCR measurement in various M17 stable cells. (**c**) Respiratory control ratio (*d/b*), (**d**) spare respiratory capacity (*d-a*) and (**e**) coupling efficiency (*c/a*) were calculated after subtracting the non-mitochondrial respiration. Data are means ± SEM of three independent experiments. Statistics: one-way analysis of variance (ANOVA) followed by Tukey's multiple comparison test. * $P < 0.05$ compared with empty-vector control (Vector); # $P < 0.05$, compared with WT.

Supplementary Figure 7. Fibroblasts from PD individual with D620N mutation demonstrate bioenergetic deficits that can be rescued by inhibition of mitochondrial fission. Bioenergetic parameters such as respiratory control ratio (**a**), spare respiratory capacity (**b**) and coupling efficiency (**c**) were measured by a seahorse XF24 analyzer in fibroblasts from PD individual bearing D620N VPS35 mutation and sex- and age-matched NHFs in the presence and absence of mdivi-1 treatment. Data are means ± SEM of three independent experiments. Statistics: one-way analysis of variance (ANOVA) followed by Tukey's multiple comparison test. * $P < 0.05$.

Supplementary Figure 8. Mitochondrial fission inhibitor, mdivi-1, does not affect the expression and phosphorylation of DLP1 in M17 cells. Representative western blots (left panel) and quantification (right panel) of DLP1 and phosphorylated DLP1 in M17 cell in the presence and absence of mdivi-1 treatment. Data are means ± SEM of three independent experiments. ns, not significant.

Supplementary Figure 9. Mitochondria fission/fusion proteins in M17 stable cell lines with manipulated expression of VPS35. (**a**) Representative western blots (left panel) and quantification (right panel, based on 3 independent experiments using 3 different clonal cell lines) of mitochondrial fission and fusion proteins in M17 cell lines stably overexpressing WT or mutant VPS35. * $P < 0.05$, compared to control cells (Ct) or vector-controls (Vec). (**b**) Representative western blot (left panel) and quantification (right panel, based on 3 independent experiments using 3 different clonal cell lines) of mitochondrial fission and fusion proteins in VPS35 KD M17 cells. * $P < 0.05$, compared to control cells (Ct) or negative-control RNAi (ncRNAi). NDUFB8 and actin were used as mitochondrial marker and internal loading control respectively. Data are means ± SEM Statistics: one-way analysis of variance (ANOVA) followed by Tukey's multiple comparison test.

Supplementary Figure 10. VPS26 and VPS35 act through the same pathway in the regulation of mitochondrial DLP1 complex turnover. (**a**) Quantification of the number of mitochondrial DLP1 puncta in fixed M17 cells: Control M17 cell or M17 cells stably overexpressing or knocking down VPS35 were co-transfected with VPS26 RNAi and mitoDsRed2. After 24 hours, cells were fixed and immunostained by anti-DLP1 antibody and the steady state levels of mitochondrial DLP1 puncta were quantified. *$P < 0.05$, compared with Control + Control RNAi cells and Vector + control RNAi cells. NS, not significant. (**b**) Western blot and quantification of DLP1 in ultracentrifugation precipitates (270K g pellets) from mitochondrial fraction of M17 stable cell lines (ncRNAi and VPS35 RNAi) with or without VPS26 RNAi treatment. *$P < 0.05$, compared with control cells without VPS26 RNAi treatment. (**c**) Western blot and quantification of DLP1 in ultracentrifugation precipitates (270K g pellets) from mitochondrial fraction of M17 stable cell lines (empty-vector control and WT VPS35 OE) with or without VPS26 RNAi treatment. *$P < 0.05$, compared with control cells without VPS26 RNAi treatment. Data

are means ± SEM from three independent experiments. Statistics: one-way analysis of variance (ANOVA) followed by Tukey's multiple comparison test.

Supplementary Figure 11. Oxidative stress increases VPS35–DLP1 interaction in M17 cells. Representative western blot (left panel) and quantification of VPS35 and DLP1 in DLP1 immunoprecipitates from M17 cells with indicated treatment. Data are means ± SEM from three independent experiments. Statistics: one-way analysis of variance (ANOVA) followed by Tukey's multiple comparison test. *$P < 0.05$.

Supplementary Figure 12. Rescuing effects of artificial VPS35 mutations on mitochondrial morphology and retromer function. Representative pictures (**a**) and quantification of mitochondrial aspect ratio (**b**) demonstrated differential rescuing effects of artificial VPS35 mutations on elongated mitochondrial morphology in VSP35 KD M17 cells: VPS35 KD M17 cells were transiently co-transfected with plasmids carrying indicated VPS35 mutation (FLAG-tagged) and mitoDsRed2 and imaged for mitochondrial morphology analysis three days later in positively-transfected cells identified by FLAG staining (green). *$P < 0.05$, compared with KD + Vector; # $P < 0.05$ compared with KD + WT. (**c**) Artificial mutations rescued retromer function in VPS35 KD M17 cells as determined by FAT/CD36 receptor recycling. FAT/CD36 receptor recycling was quantified in VPS35 KD M17 cells transiently transfected with artificial VPS35 mutants as identified by FLAG staining. *$P < 0.05$, compared with empty-vector control cells (Control). Data are means ± SEM from three independent experiments. Statistics: one-way analysis of variance (ANOVA) followed by Tukey's multiple comparison test.

Supplementary Figure 13. Specificity of DLP1 antibody. Western blot of DLP1 in the total lysate from human fibroblasts demonstrated the specificity of the DLP1 antibody. Similar results were obtained for M17 cells and primary neurons (not shown).

.

Supplementary Figure 14. Peroxisomal DLP1 is not changed by VPS35 overexpression or knockdown. Control M17 cells or stable clonal M17 cells with manipulated VPS35 expression were seeded in the glass chamber slides and stained by anti-DLP1(green) and anti-PEX19 (peroxisome marker, red) antibodies. Representative confocal images (**a**) and line scan analysis by ImageJ (**b**) of the fluorescence profile revealed no significant difference of the intensity of DLP1 on peroxisome between

various M17 stable cell lines with different VPS35 manipulations. Data are means ± SEM from three independent experiments. Statistics: one-way analysis of variance (ANOVA) followed by Tukey's multiple comparison test.

Supplementary Figure 15. Schematic representation of the role of VPS35/retromer in the regulation of mitochondrial dynamics by mediating the turnover of mitochondrial DLP1 complex through MDVs. Oligomeric DLP1 complexes remain on daughter mitochondria after fission which are likely inactive and become inhibitory to subsequent fission either due to the occupancy of fission sites, sequestration of DLP1 recruiting factors, and/or spatial blockage. On these daughter mitochondria, retromer recognizes and binds to mitochondrial DLP1 complex (i.e., oligomer DLP1) through VPS35–DLP1 interaction (step ①) and mediates the formation of TOM20-positive/mitoDsRed2-negative MDVs containing the DLP1 complex (step ②). DLP1 complex-containing MDVs become pinched off from mitochondria and trafficked (step ③) to lysosome (step ④) where DLP1 complexes are degraded (step ⑤). This VPS35-mediated turnover of mitochondrial DLP1 complex is a critical process required for efficient mitochondrial fission. In Parkinson disease, increased VPS35–DLP1 interaction either due to PD-associated VPS35 mutations (familial PD) or due to oxidative modifications (as seen in sporadic PD) leads to enhanced recycling of mitochondrial DLP1 complexes and increased mitochondrial recruitment of fission-competent DLP1 species which tips the balance towards more efficient fission and results in mitochondrial fragmentation and functional deficits. In VPS35 knockdown cells, reduced levels of VPS35 slow down the recycling of mitochondrial DLP1 complexes which inhibits fission and leads to elongated mitochondria.